

# Synthesis of Mesoporous TiO<sub>2</sub> and Its Application to Photocatalytic Activation of Methylene Blue and *E. coli*

Eun-Young Kim, Dong Suk Kim,<sup>†</sup> and Byung-Tae Ahn<sup>\*</sup>

Department of Chemistry, Ewha Womans University, Seoul 120-750, Korea. \*E-mail: btahn@mm.ewha.ac.kr

<sup>†</sup>Korean Agency for Technology and Standards, Gwacheon 427-723, Korea

Received April 28, 2008, Accepted November 24, 2008

Mesoporous TiO<sub>2</sub> material was synthesized from diblock copolymers with ethylene oxide chains via a sol-gel process in aqueous solution. The properties of these materials were characterized with several analytical techniques including field emission scanning electron microscopy (FE-SEM), transmission electron microscopy (TEM), wide angle X-ray diffraction (XRD), Brunauer-Emmett-Teller (BET) analysis, and Barrett-Joyner-Halenda (BJH) analysis. The mesoporous TiO<sub>2</sub> materials calcined at 400°C were found to have specific surface areas 212 m<sup>2</sup> g<sup>-1</sup>, average pore sizes 6.2 nm, and their average crystal sizes were found to be 8.2 nm. The photocatalytic activity of mesoporous TiO<sub>2</sub> was characterized with UV-Vis spectroscopy, and it was found to be 5.8 times higher than that of Degussa P25 TiO<sub>2</sub> (P25). For deactivation of *Escherichia coli*, mesoporous TiO<sub>2</sub> also has high photocatalytic inactivity than that of P25. Such a high photocatalytic activity is explained with large surface area and small crystal size with wormhole-like mesoporous structure.

**Key Words:** Synthesis, Mesoporous TiO<sub>2</sub>, Photocatalytic degradation, Inactivation, *E. coli*

## Introduction

Titanium dioxide (TiO<sub>2</sub>) is a semiconductor with a large band gap of 3.2 eV, which can produce the hydroxyl radical and super oxide under UV irradiation.<sup>1-3</sup> Such properties allow their utilizations for key materials as photocatalyst, dye-sensitized solar cells (DSSCs), photochromic devices and environmental pollution reducers.<sup>4,6</sup> The photocatalytic activity of TiO<sub>2</sub> has been considered to be determined by the crystalline phase, crystal size, and specific surface area. To improve the photocatalytic activity of TiO<sub>2</sub>, small size and high crystallinity of nanoparticles have been used. Small crystal size can lead to quantum size effect in semiconductor.<sup>7-9</sup> Due to active site number, TiO<sub>2</sub> with a large surface area is expected to exhibit outstanding photochemical activity.

Mesoporous TiO<sub>2</sub> has a large surface area because of its confined porous structure and high surface to volume ratio, and so it should in principle have high photochemical sterilization, because of the improved access to the active sites of TiO<sub>2</sub>.<sup>10-12</sup> However, much less research has been devoted to improving the photocatalytic activation of mesoporous TiO<sub>2</sub> compared to that invested in nonporous or commercial TiO<sub>2</sub>. The low crystallinity of mesoporous TiO<sub>2</sub> with an amorphous or semicrystalline framework is thought to be the main reason for its negligible photocatalytic activity. Increasing the crystallinity through calcination at high temperatures is not expected to be helpful because of the resulting collapse of the mesoporous framework and the consequent loss of surface area.

In this study, we report the synthesis of mesoporous TiO<sub>2</sub> through the sol-gel approach of titanium (IV) precursor containing block copolymer in water solution. The resulting materials have the spherical morphology via aggregation of anatase phase single crystalline particles with large surface area and high crystallinity. Owing to their specific physical properties, the photocatalytic degradation of methylene blue and

photochemical sterilization of mesoporous TiO<sub>2</sub> is significantly higher than that of P25.

## Experiment

**Synthesis of mesoporous TiO<sub>2</sub>.** Titanium tetraisopropoxide (Ti(O<sup>i</sup>Pr)<sub>4</sub>, 97%, Aldrich) and the diblock copolymer surfactants Lutensol AT 50 (C<sub>16</sub>C<sub>18</sub> fatty alcohol and 50 of PEO units) were used without further purification. 3 g of surfactant (1.2 mmol) was dissolved in 100 mL of distilled water, and then 1.5 g (15.3 mmol) of concentration 95% sulfuric acid was added. Next, titanium tetraisopropoxide (27.5 mmol) mixed with 2,4-pentanedione (27.5 mmol) was dropped into surfactant solution under magnetic stirring. The resulting solutions were kept at 50°C for 10 h and then hydrothermal treatment was carried out at 90°C for about 24 h. The solids in the solutions were filtered out, dried in air. Finally, the material was calcined at 400°C at a rate of 1°C min<sup>-1</sup> in air.

**Characterization.** The Field emission-gun scanning electron microscope (FE-SEM, JEOL JSM-6330F) and transmission electron microscope (TEM, JEOL JEM-2000EXII) was used to determine the morphology and pore structure of the mesoporous TiO<sub>2</sub> particle. X-ray diffraction (XRD, MAC/Sci. MXP 18XHF-22SRA with Cu K $\alpha$  radiation) was used to survey the crystal compositions and crystal sizes. The crystal size was calculated with the Scherrer equation ( $\Phi = K\lambda/\beta\cos\theta$ ), where  $\Phi$  is the crystal size,  $K$  is usually taken as 0.89,  $\lambda$  is 0.154 nm, which is the wavelength of the X-ray radiation,  $\beta$  is the full width at half maximum intensity (FWHM), and  $\theta$  is the diffraction angle of the {101} peak for anatase ( $2\theta = 25.3^\circ$ ). The surface area and pore size distribution was investigated with BET and BJH analysis with a Micrometrics ASAP 2000 apparatus after the samples were degassed at 200°C for 10 h. The specific surface areas were estimated by using the Brunauer-Emmett-Teller (BET) method, and the pore size distributions

were determined with the Barrett-Joyner-Halenda (BJH) method by using the nitrogen desorption branches of the isotherms.

**Photocatalytic degradation of methylene blue.** The photocatalytic activity of the mesoporous TiO<sub>2</sub> sample was investigated by measuring the degradation of methylene blue (MB) with UV-irradiation, and compared with that of P25. Quartz cell contained 20 mL of the aqueous 50 ppm MB solution and 20 mg of the catalyst. In order to provide sufficient UV radiation, four UV-A (20W) lamps which the wavelengths range between 320 and 400 nm were used as light sources. After 30 min stirring in dark, the solution was then irradiated under UV light with continuous magnetic stirring. A fixed quantity of each MB solution was taken at regular intervals during the irradiation time and filtered through a syringe filter to evaluate the concentration of MB remaining in the solution. The UV-Vis absorption spectra of the taken solutions were obtained using a Shimadzu 2101PC UV-Vis scanning spectrophotometer in the range 500-700 nm ( $\lambda_{\text{max.}} = 664$  nm for methylene blue)

**Photocatalytic inactivation of *E. Coli*.** *Preparation of mesoporous TiO<sub>2</sub> thin film:* To make TiO<sub>2</sub> thin film, doctor-blade coating system was used. In mortar, 420  $\mu\text{L}$  of 2,4-pentanedione (0.1 M) was dropped into 1.2 g of mesoporous TiO<sub>2</sub> and mixed vigorously for 30 min until homogeneity obtained. And then, each 500  $\mu\text{L}$  of distilled water was added 3 times with vigorously mixing. After 0.24 g of PEO (MW. 10,000) was mixed, 0.24g of PEG (MW. 100,000) was mixed step by step. The viscous suspension was spread onto a glass plate (5 cm  $\times$  5 cm) at room temperature using adhesive tape as a spacer to obtain a unique film thickness. After that, the mixed solution was coated with screen printing method.<sup>13</sup>

*Culture of micro-organism: Escherichia coli (E. coli)* was used as standard micro-organism. The initial concentration of *E. coli* was  $\sim 10^6$  cells/mL. The 0.5 mL of this solution was used as a test inoculum.

*Photocatalytic reaction procedure:* Before photocatalytic inactivation test, the mesoporous TiO<sub>2</sub> coated sample was washed with 70% ethanol. Then the test pieces was put under UV light (BLB lamp, 1.0 mWcm<sup>-2</sup>) to initiate the photocatalytic activity. The 0.5 mL of  $\sim 10^6$  cells/mL suspension was dropped on the mesoporous TiO<sub>2</sub> coated sample, and the sterilized polyethylene film which was cut 5 $\times$ 5 cm was covered on it. After UV-A irradiation (intensity is 1.0 mWcm<sup>-2</sup>), the sample was taken at regular intervals during the illumination period. For evaluation of inoculated bacteria, add 4.5 mL of neutralization solution, massage the sample, and wash the covering film sufficiently with pipette. 1 mL of solution was withdrawn with pipette and diluted 10-fold serially with phosphate buffered physiological saline. Dilution ranged from 10<sup>0</sup> to 10<sup>2</sup> is suitable. Finally 0.1 mL sample of the diluted solutions was spread in order to count the number of colonies. The number of colony forming units (CFUs) is determined after 24 h incubation at 37°C.

## Result And Discussion

**SEM and TEM Images Analyses.** Figure 1 shows the FE-SEM and HR-TEM images of mesoporous TiO<sub>2</sub> calcined at 400°C. The morphology of synthesized material has spherical shape and its diameter was approx. 2  $\mu\text{m}$  as shown in Figure

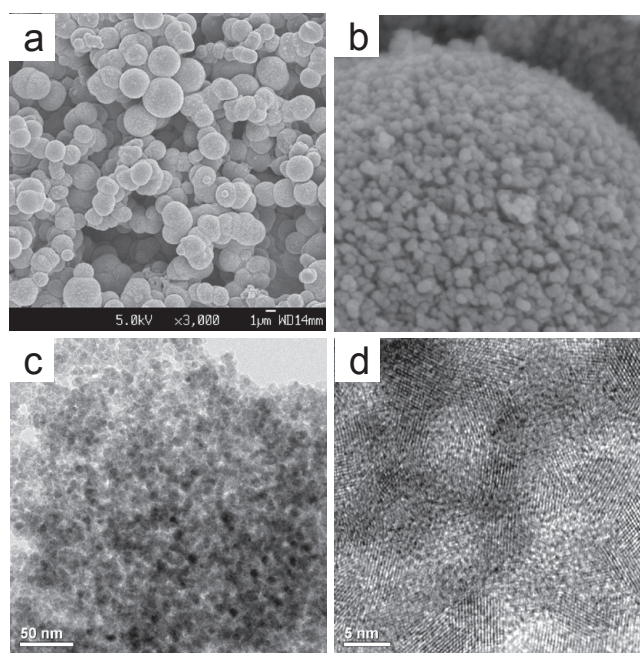


**Figure 1.** FE-SEM image of synthesized mesoporous (a), and a magnified FE-SEM image of a selected area of one particle (b). HR-TEM image of mesoporous TiO<sub>2</sub> (c), and a magnified image of nanocrystalline anatase (d).

1a. Such a spherical shape of mesoporous TiO<sub>2</sub> can be expected to induce the surface tension of surfactant through sol-gel process. To survey whether the synthesized material has porous structure or not, the magnified FE-SEM image of the one particle is investigated. It is observed that the discernable pore are present at the surface of mesoporous TiO<sub>2</sub>, and the pore structure consists of a wormhole-like pore array as shown in Figure 2b. Approx. 10 nm of numerous TiO<sub>2</sub> nanoparticles are aggregated and approx. 2  $\mu\text{m}$  size of mesoporous TiO<sub>2</sub> is synthesized. The FE-SEM images also show the evidence for disordered, wormhole-like framework pore structure. To observe the pore size and its array of mesoporous TiO<sub>2</sub>, HR-TEM images of the mesoporous TiO<sub>2</sub> were investigated as shown in Figure 1c and 1d. The observable site shows that the pore structures are spotted with a non-ordered worm-hole like

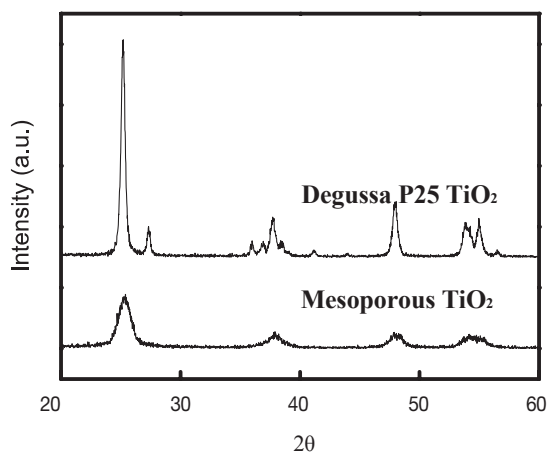


**Figure 2.** Wide angle X-ray diffraction patterns at different temperature: as-synthesized, calcined at 400°C and P25.

structure as shown in Figure 1c. The pore structure is observed at the space between TiO<sub>2</sub> nanoparticles, indicating the interparticle porosity is due to the mesoporosity. This result is consistent with the SEM image. The pore size of mesoporous TiO<sub>2</sub> is estimated about 6 nm. On the further magnified HR-TEM image, aggregated numerous nanocrystalline TiO<sub>2</sub> nanoparticles and mesopore structures formed were shown as in Figure 1d. The crystal phase of anatase structure is induced and its average crystal size is about 8 nm.

From the FE-SEM and HR-TEM analyses, the mechanism for the formation of mesoporous TiO<sub>2</sub> can be analogized. As can be seen from the FE-SEM and HR-TEM images, the mesoporous TiO<sub>2</sub> probably arises from the aggregation of nanocrystalline TiO<sub>2</sub> particles. When the titanium precursor was dissolved in surfactant solution, TiO<sub>2</sub> nanoparticles can be formed via hydrolysis and condensation of precursor, and interaction with the hydrophilic PEO blocks of surfactant micelle only. At this state, the formed TiO<sub>2</sub> nanoparticles are stabilized with surfactant micelle. Further hydrolysis and condensation of titanium precursors lead to the growth of larger TiO<sub>2</sub> nanoparticles, which are slowly aggregated to one another. As TiO<sub>2</sub> nanoparticles are further aggregated, the TiO<sub>2</sub> particles become microscopic particles, and finally form microspheres as shown Figure 1 images. Similar aggregation of nanoparticles leading to mesoporous sphere was also studied by Zhou *et al.* and Yang *et al.*<sup>14-15</sup>

**XRD Analysis.** To determine the TiO<sub>2</sub> crystal composition, wide angle X-ray diffraction patterns were measured as shown in Figure 2. In case of mesoporous TiO<sub>2</sub> calcined at 400°C, the broaden diffraction peak of anatase is observed and the crystal size calculated by the Scherrer equation formula from anatase peak {101} is about 8.2 nm. This result is similar with the HR-TEM image of Figure 1d. On the other hand, the diffraction peak of P25 has anatase and rutile structure, and its crystal size is approx 25 nm, which is similar result with reference data of P25.<sup>16</sup>

**BET and BJH Analyses.** The specific surface area and porosity of the mesoporous TiO<sub>2</sub> were investigated by using the N<sub>2</sub> adsorption and desorption isotherms before and after the calcination as shown in Figure 3. All the isotherms of samples reveal the stepwise adsorption and desorption branch of type IV curves, indicating the presence of mesoporous material having a three dimensional (3D) intersection according to the IUPAC classification. A hysteresis loop with a stepwise adsorption and desorption branch is observed at wide range of pressure (P/P<sub>0</sub>), and the surface area of mesoporous TiO<sub>2</sub> calcined at 400°C is 212 m<sup>2</sup>g<sup>-1</sup> as shown in Figure 3a. However, a hysteresis loop with a stepwise adsorption and desorption branch is not observed in case of P25. The surface area is 50 m<sup>2</sup>g<sup>-1</sup> as shown in Figure 3a. This result indicates that the synthesized material has wider mesoporous structure. To analysis pore size and pore volume, the plots of the pore size distribution are investigated by desorption branch of the BJH method as shown in Figure 3b. The average pore diameter of mesoporous TiO<sub>2</sub> calcined at 400°C is 6.2 nm with relatively narrow pore size distribution. The pore volume of mesoporous TiO<sub>2</sub> is 0.4 cm<sup>3</sup>g<sup>-1</sup>. However, the pore size distribution of P25 is not observed and pore volume is not also counted. Such a

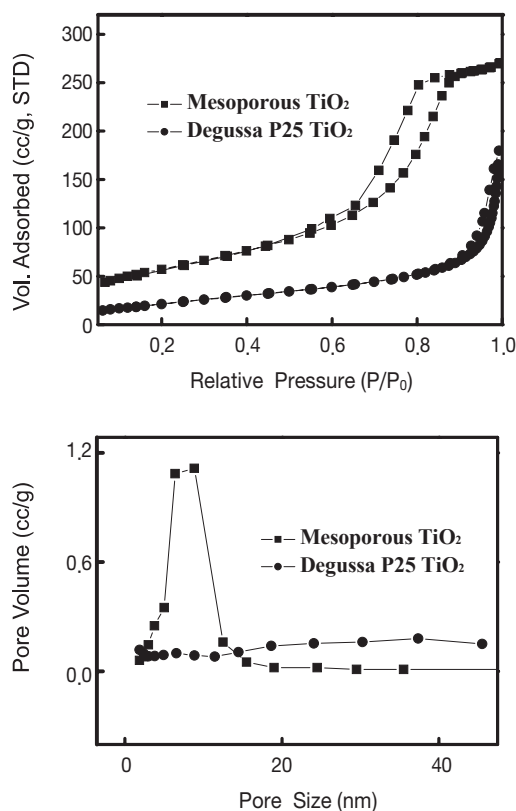


**Figure 3.** Nitrogen adsorption and desorption isotherms of mesoporous TiO<sub>2</sub> and Degussa P25 TiO<sub>2</sub> (a). The pore size distributions of mesoporous TiO<sub>2</sub> and P25 (b).

physical properties of large surface area and high crystallinity with nanocrystalline aggregated is good candidate material for high photocatalytic activity.

**Photocatalytic Degradation of Methylene Blue.** The photocatalytic activity of mesoporous TiO<sub>2</sub> was carried out by the degradation of methylene blue solution under UV-irradiation as shown in Figure 4. That of the mesoporous TiO<sub>2</sub> was higher than that of commercial TiO<sub>2</sub> P25. For the 400°C calcined mesoporous TiO<sub>2</sub>, the methylene blue was almost all degraded within 30 min under UV-irradiation, whereas the degradation time of commercial TiO<sub>2</sub> P25 took about 60 min for 90% degradation of methylene blue. A plot of ln(C<sub>0</sub>/C) versus UV irradiation time, the slopes of straight lines were represented in all materials, indicating that the degradation rate of methylene blue followed the first order process. The higher photocatalytic activity of mesoporous TiO<sub>2</sub> can be explained in terms of its large surface area and small crystal size. A larger surface area is likely to result in better photocatalytic activity, because a larger surface area provides more active sites. These mesoporous TiO<sub>2</sub> materials have larger surface areas (approx. 212 m<sup>2</sup>g<sup>-1</sup>) than the P25 (approx. 50 m<sup>2</sup>g<sup>-1</sup>). Therefore, mesoporous TiO<sub>2</sub> is likely to have better photocatalytic activity than the P25. Another factor that influences photocatalytic activity is crystal size. It is commonly accepted that a smaller crystal size corresponds to more powerful redox ability because smaller crystal induce a larger band gap due to the quantum size effect, which arises due to a dramatic reduction

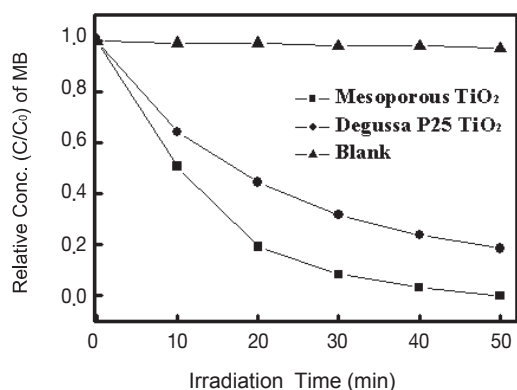


**Figure 4.** The relative concentrations of methylene blue (MB) as functions of UV irradiation time in the presence of mesoporous TiO<sub>2</sub> and P25.

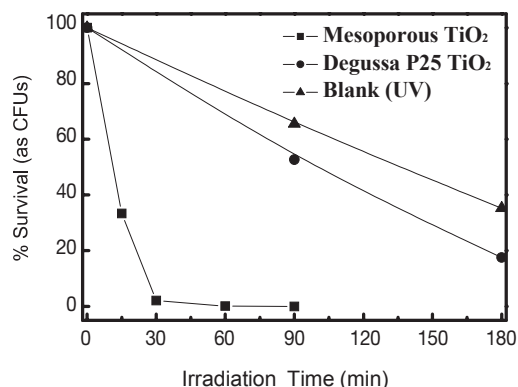


**Figure 5.** The concentrations of *E. coli* as functions of UV irradiation time in the presence of mesoporous TiO<sub>2</sub> and P25.

in the number of free electrons. Since the mesoporous TiO<sub>2</sub> was formed by the aggregation of nanocrystalline anatase with a smaller crystal size (approx. 8.2 nm) than that of P25 (approx. 25 nm), its photocatalytic activity is better.

**Photocatalytic Inactivation of *E. coli* Disinfection.** The performance of mesoporous TiO<sub>2</sub> as a photocatalyst is demonstrated using a Film adhesion method in a recirculating air experimental facility. *Escherichia coli* was used as index to demonstrate the disinfection efficiency of the photocatalysis process. Antibacterial activity is measured by quantifying the survival of bacterial cells which have been held in intimate contact for 60 min at RT with a surface containing a mesoporous TiO<sub>2</sub> or P25. The antibacterial effect is measured by comparing the survival of bacteria on a TiO<sub>2</sub> coated surface with that achieved on an uncoated surface. Figure 5 shows that of mesoporous TiO<sub>2</sub> coated surface, P25 coated surface, and uncoated surface under UV-A irradiation. At same photocatalytic degradation experiment of methylene blue, a relatively high rate of bacterial inactivation was observed for mesoporous TiO<sub>2</sub> coated sample, whereas a relatively low rate of bacterial inactivation was observed for P25 coated sample. When the bacteria were exposed to TiO<sub>2</sub> in the dark no reduction in viable counts was observed. In the case of the P25 sam-

ple, the efficacy of *E. coli* inactivation reached 48% in 90 min. However, in the case of the mesoporous TiO<sub>2</sub> coated sample, the *E. coli* bacteria cells were inactivated completely (approx. 98.5%) within 30 min of UV irradiation. These results indicate that the mesoporous TiO<sub>2</sub> has high photocatalytic activity of methylene blue degradation as well as bacteria disinfection. Such high photocatalytic disinfection also is explained due to the large surface area and small crystal size of mesoporous TiO<sub>2</sub>. The bacteria were contacted with large surface area of mesoporous TiO<sub>2</sub> and easily contact the OH radical induced UV-A irradiation, and consequently high reduction in bacterial number was observed. Furthermore, the small crystal size and high crystallinity of mesoporous TiO<sub>2</sub> give more chance to make high concentration of OH radical on the TiO<sub>2</sub> coated sample. Therefore, the photocatalytic disinfection of mesoporous TiO<sub>2</sub> has higher than that of P25.

## Conclusion

This study has shown that mesoporous TiO<sub>2</sub> can be successfully synthesized with a sol-gel approach from a mixture of a block copolymer and a titanium precursor in aqueous solution. 450 °C calcined sample was approx. 2 μm, surface area : 212 m<sup>2</sup>g<sup>-1</sup>, pore size : 6.2 nm, and crystal size : 8.2 nm. The mesoporous TiO<sub>2</sub> was found to exhibit higher photocatalytic activities in the degradations of methylene blue than the P25, indicating that the mesoporous TiO<sub>2</sub> can be effectively used in photocatalysis. In addition, the photocatalytic disinfection of bacteria also has higher reduction that nonporous TiO<sub>2</sub> sample.

## References

- Huang, Z.; Maness, P. C.; Blake, D. M.; Wolfrum, E. J.; Smolinski, S. L.; Jacoby, W. A. *J. Photochem. Photobiol. A* **2000**, *130*, 163-170.
- Cho, M.; Chung, H.; Choi, W.; Yoon, J. *Water Res.* **2004**, *38*, 1069-1077.
- Fu, G.; Vary, P. S.; Lin, C. T. *J. Phys. Chem. B* **2005**, *109*, 8889-8898.
- Calleja, G.; Serrano, D. P.; Sanz, R.; Pizzaro, P.; Garcia, A. *Ind. Eng. Chem. Res.* **2004**, *43*, 2485-2492.
- Hoffmann, M. R.; Martin, S. T.; Choi, W.; Bahnemann, D. W. *Chem. Rev.* **1995**, *95*, 69-96.
- Stone, V. F.; Davis, R. J. *Chem. Mater.* **1998**, *10*, 1468-1474.
- Antonelli, D. M.; Ying, J. Y. *Angew. Chem. Int. Ed. Engl.* **1995**, *34*, 2014-2017.
- Kresge, C. T.; Leonowicz, M. E.; Roth, W. J.; Vartuli, J. C.; Beck, J. S. *Nature* **1992**, *359*, 710-712.
- Zhang, Y.; Weidenkaff, A.; Reller, A. *Mater. Lett.* **2002**, *54*, 375-381.
- Zhan, S.; Chen, D.; Jiao, X.; Tao, C. *J. Phys. Chem. B* **2006**, *110*, 1199-11204.
- Peng, T.; Zhao, D.; Dai, K.; Shi, W.; Hirao, K. *J. Phys. Chem. B* **2005**, *109*, 4947-4952.
- Kim, D. S.; Kwak, S. Y. *Appl. Catal. A* **2007**, *323*, 110-118.
- Yanagida, H.; Takata, M.; Nagai, M. *J. Am. Ceram. Soc.* **1981**, *64*, 34-35.
- Zhou, Y.; Antonietti, M. *J. Am. Chem. Soc.* **2003**, *125*, 14960.
- Yang, H. G.; Zeng, H. C. *J. Phys. Chem. B* **2004**, *108*, 3492.
- Ma, Y.; Yao, J. *Chemosphere* **1999**, *38*, 2407.